Korean J. Chem. Eng., **31**(6), 961-971 (2014)
DOI: 10.1007/s11814-014-0008-4

pISSN: 0256-1115
eISSN: 1975-7220

Tungsten oxides supported on nano-size zirconia for cyclic production of syngas and hydrogen by redox operations

Jung Hun Kwak‡, Gui Young Han, Jong Wook Bae, and Ki June Yoon†

School of Chemical Engineering, Sungkyunkwan University (SKKU),
2066 Seobu-ro, Jangan-gu, Suwon-si, Gyeonggi-do 440-746, Korea
(*Received 1 October 2013 • accepted 6 January 2014*)

Abstract−For cyclic production of syngas and H_2 by redox (methane reforming-water splitting) operations, samples of tungsten oxides supported on nano-size zirconia (WO_3/n-ZrO_2) were investigated at 1,223 and 1,273 K and compared with those on micron-size zirconia (WO_3/μ-ZrO_2). The reduction characteristics of WO_3/n-ZrO_2 observed in this study were consistent with those of WO_3/μ-ZrO_2 reported in the literature. Specifically, the reduction process comprised three stages, the syngas production rate decreased as WO_3 content increased, and the overall degree of reduction gradually decreased with repeated cycles. However, there were differences due to the smaller particle size, namely, WO_3/n-ZrO_2 yielded a higher syngas production rate and a lower $H_2/(CO+CO_2)$ ratio. In addition, the hydrogen yield by water splitting was significantly lower than the amount expected based on the overall degree of WO_3 reduction. The $H_2/(CO+CO_2)$ ratio also gradually decreased with repeated cycles. These results were mainly attributed to rapid sintering of WO_3/n-ZrO_2, which gradually began to resemble WO_3/μ-ZrO_2.

Keywords: Hydrogen, Nano-size Zirconia, Methane Reforming, Syngas, Tungsten Oxide

INTRODUCTION

A study on tungsten oxides supported on micron-size zirconia for cyclic production of syngas and H_2 by methane reforming (reduction) and water splitting (re-oxidation) was recently reported by the authors [1]. The main findings of this study were as follows: (i) WO_3 is reduced to WO_2 in the first stage of reduction with negligible metallic W formation, and further reduced to W in the second reduction stage; (ii) in addition to the main reductant, methane, H_2 and CO in the produced syngas can also reduce significant portions of WO_3 and WO_2, the degrees of reduction of which were determined and compared; (iii) deposition of carbon formed by methane decomposition can be avoided by using an appropriate operation time at a given temperature; (iv) the effects of the reduction temperature and content of WO_3 supported on micron-size zirconia on the overall degree of WO_3 reduction were established, and the $H_2/(CO+CO_2)$ ratio in the syngas and the reduction rates were compared; and (v) during repeated cyclic operations, the syngas and H_2 yields decrease. As a continuation of this previous study, we focused on the effects of particle size of nano-size zirconia support on the degree of reduction, syngas $H_2/(CO+CO_2)$ ratio, reduction rate, and stability of samples during repeated cyclic operations.

There is growing interest in storage of solar energy in chemicals obtained by endothermic reactions as an important technology for sustainable energy [2,3]. For this purpose, various solar thermochemical processes have been proposed to produce hydrogen which is the most desirable energy resource obtainable from water. Among these processes, cyclic redox consisting of thermal reduction and water splitting has been investigated extensively. The first step of this process is reduction of metal oxides at a high temperature accompanied by liberation of oxygen, while the second step is re-oxidation of the reduced metal oxide or metal by water with liberation of hydrogen [4]. Existing redox systems have several problems, including a very high temperature requirement (>2,100 K) for thermal reduction [5-8] and poor H_2 yields in the re-oxidation step [6]. Thus, several investigators have reported promising systems that show reasonable reactivity at 1,673-1,773 K and good repeatability during repeated cyclic operations, with examples including ZrO_2-supported ferrites [9,10] and cerium oxide mixed with ZrO_2, NiO, and Ta_2O_5 [11,12].

The temperature range noted above is still considered to be too high, and reducing agents can be used to further lower the temperature of oxide reduction. The reducing agents that have been used include coal [3,13] and CO [14-16]; for example, iron oxides can be effectively reduced by CO below 1,123 K. However, the most widely investigated reducing agent is methane, which is more readily available from natural gas, the use of which allows reduction to take place below 1,300 K [17-28]. In this process, the first step is reduction of a metal oxide by methane to produce syngas (methane reforming step), while the second step involves re-oxidation of the reduced metal oxide or metal by water to produce hydrogen (water splitting step). The re-oxidized metal oxide can then be reused in the first step, thus constituting a cyclic operation [24]. However, other competing reactions can take place in addition to the cyclic reactions described above. Among the possible competing reactions, major side reactions during the methane reforming step are metal oxide reduction by hydrogen and CO in the syngas, methane decomposition to produce deposited carbon, and carbide formation

†To whom correspondence should be addressed.
E-mail: kijyoon@skku.edu
‡Present address: OCI Materials Co., Ltd., R&D Center, 60-5, Sangjuldong, Yeongju, Gyeongbuk 750-080, Korea.

[1,21,24,28]. These competing reactions cause the syngas yield to decrease and the H_2/CO ratio in the syngas to deviate from a value of 2, although the ratio of 2 is preferred for subsequent methanol synthesis or the Fischer-Tropsch synthesis. In addition, the hydrogen produced during the water splitting step may be contaminated with carbon oxides due to the deposited carbon or metal carbide; however, this can be avoided by carefully controlling the operating temperature and reaction duration [1,24].

Numerous metal oxides have been investigated for the two-step process described above: Fe_3O_4 [17], ZnO [7,18], CeO_2-ZrO_2 composite oxides [19], Ni-, Co-, Zn-, Mn- and Cu-ferrites [20-23], CeO_2 [24], SnO_2, In_2O_3, MoO_2, V_2O_5 [25-27], and WO_3 [1,25-27]. Among these, WO_3 is especially interesting because all lattice oxygen in WO_3 can be utilized; that is, WO_3 is first reduced to WO_2, which is further reduced to metallic W. Moreover, it can be reduced relatively fast at around 1,223 K and the high melting point of WO_3 systems provides good resistance to sintering, which allows for stable repeated cyclic operations [1,27].

Sintering of metal oxides during repeated cycling is an additional inevitable problem, but one that can be minimized by using supports such as ZrO_2, CeO_2, and ceria-zirconia composites [1,14, 23-28]. Previous studies have primarily relied upon micron-size support particles. In the present study, the support material employed instead was nano-size zirconia, by which it is expected that the overall degree of WO_3 reduction and the reduction rates would be improved. The effects on the syngas H_2/CO ratio and stability of samples during repeated cyclic operations were also investigated. Apart from the preparation of nano-size ZrO_2, the experimental and analysis procedures were similar to those in our previous study [1].

EXPERIMENTAL

1. Preparation of Nano-size ZrO_2

A nano-size zirconia support (n-ZrO_2) was prepared from an electrolyte mixture resulting from anodization of Zr foils [29]. The anodization and n-ZrO_2 preparation procedure used in this study were established in our laboratory by combining and modifying previously described procedures for preparation of TiO_2 and ZrO_2 nanotubes [30,31]. The primary purpose of anodization of Zr foils was to obtain ZrO_2 nanotubes; however, the yield of ZrO_2 nanotubes was usually below 20%, and the remaining electrolyte mixture contained about 80% of the original Zr in the forms of ionic species of Zr such as $[ZrCl_6]^{2-}$ and $[ZrOCl_4]^{2-}$ and very fine suspended precipitates such as $Zr(OH)_xO_y$ [30-32]. Therefore, the mixture resulting after anodization was used to recover Zr compounds in the form of n-ZrO_2.

Zr foil (Alfa Aesar, 99% purity, 40 mm×40 mm×0.25 mm) was cleaned by sonication in deionized water and then in acetone, after which it was dried in ambient air. An electrolyte solution was prepared from deionized water and perchloric acid ($HClO_4$: Samchun Pure Chemical, 60% assay) to form a 0.2-molar solution. Anodization was performed with a cleaned Zr foil at the anode and a platinum mesh at the cathode by immersing a half height of the two electrodes into the electrolyte while stirring with a magnetic bar at a constant potential of 20 V applied with a potentiostat. During anodization, the electrolyte temperature was gradually increased due to anodization of Zr and electrical resistance. Therefore, anodization was stopped when the temperature reached 313 K and the electrolyte solution was replaced with a fresh solution at room temperature to avoid excess temperature and accelerate the anodization process. Anodization was continued until the immersed portion of the foil began to disintegrate. The resulting electrolyte mixture was filtered, and the filter cake, which consisted primarily of agglomerates of ZrO_2 nanotubes, was washed with deionized water and dried in a drying oven at 353 K overnight to obtain ZrO_2 nanotubes. The obtained ZrO_2 nanotubes were then employed as a support for WO_3. However, the redox performance of the WO_3 on ZrO_2 nanotubes was not improved compared with the WO_3 on micron-size ZrO_2 (WO_3/μ-ZrO_2) [1,29]. Therefore, further experiments with WO_3 on ZrO_2 nanotubes were not performed.

To obtain n-ZrO_2, a sufficient volume of a 0.2-N NaOH solution was added to the filtrate containing dissolved ionic Zr species and very fine Zr-derived precipitates. The precipitates were then filtered, washed several times with deionized water, dried at 353 K overnight, and calcined at 673 K for 6 h. The size of the obtained n-ZrO_2 particles was 10-30 nm, and the specific surface area was 51.6 m^2/g, which was significantly higher than the 6.4 m^2/g surface area of μ-ZrO_2 [1].

2. Preparation of WO_3 Supported on n-ZrO_2

Samples of WO_3 supported on n-ZrO_2 (WO_3/n-ZrO_2) were prepared by following the procedures detailed in our previous study [1]. Briefly, n-ZrO_2 powder was added to an aqueous solution of $(NH_4)_6H_2W_{12}O_{40}$ (Fluka, 99% purity). The solution was then evaporated to dryness while stirring at 343-353 K for one day, followed by calcination in air at 1,173 K for 2 h. The calcined solid was then crushed and sieved to obtain powder samples 106-250 μm in size. The content of WO_3 in the samples was adjusted to 10, 30, or 50 wt% using predetermined amounts of material.

3. Temperature-programmed-reduction (TPR) Experiments

Samples were first investigated by TPR experiments to obtain preliminary data on the extent of reduction by both the main reaction and competing reactions and provide an overview of the reduction characteristics. The TPR apparatus shown in Fig. 1 was essentially the same as reported in our previous study [1], except that the sample holding zone was ball-shaped with a diameter of 20 mm, which ensured that the decrease and fluctuations in pressure were significantly reduced. Experimental procedures for operating the TPR apparatus were as previously described [1]. Briefly, the WO_3/n-ZrO_2 sample was packed between quartz wool in the sample holding zone, and one gram of the sample was generally used. The feed rates of CH_4 and N_2 were 1.5 and 13.5 cm^3 (STP)/min, respectively. According to programmed ramp rates, the temperature of the reactor was increased from room temperature to 1,273 K. The effluent gas from the reactor was analyzed with two gas chromatographs: one equipped with a Carboxen 1000 column (Supelco, US) using Ar as the carrier gas for the analysis of H_2, N_2, CO and CH_4, and the other equipped with a Hayesep Q column (Supelco, US) using He as the carrier gas, for specific analysis of (N_2+CO), CH_4, and CO_2. The amounts of H_2, N_2, CO, CH_4 and CO_2 were determined with a thermal conductivity detector using calibrated data for the given carrier gas.

4. Methane Reforming-water Splitting Cyclic Operations

Methane reforming-water splitting cyclic operations were performed by following the same procedure described in our previous

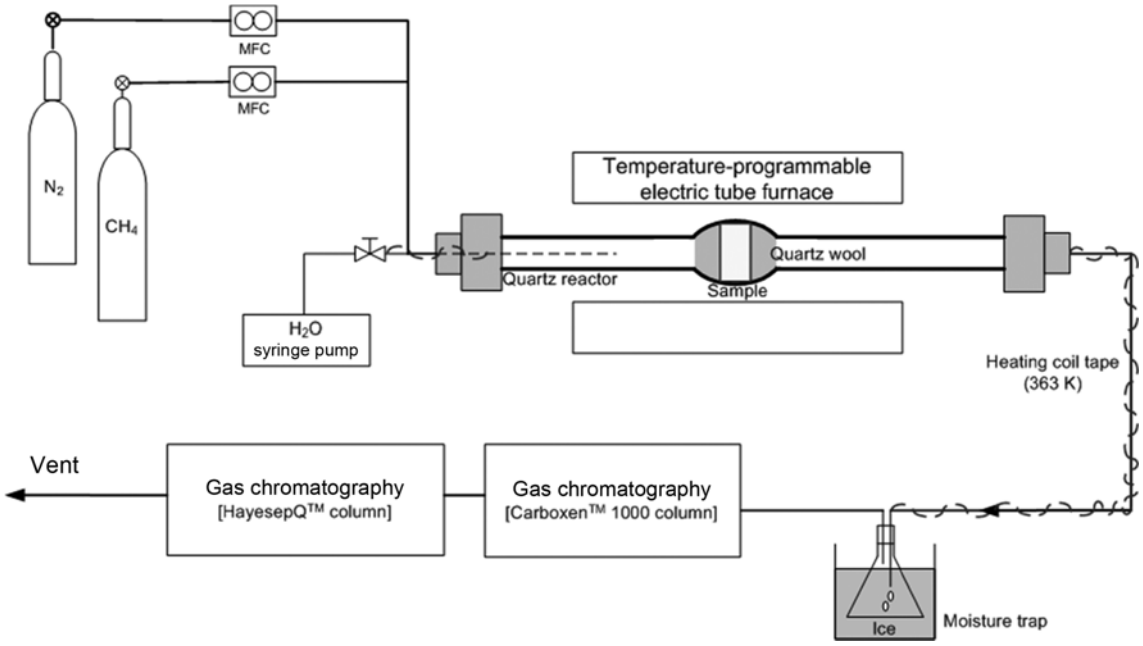

Fig. 1. Schematic diagram of the apparatus for TPR and cyclic operations.

study [1] at two fixed temperatures (1,223 and 1,273 K) with the same apparatus shown in Fig. 1. After the desired temperature was reached while flushing the reactor with N_2, the methane reforming experiment was initiated by feeding CH_4 into the reactor. The flow rates of CH_4 and N_2 were the same as in the TPR experiment. At a predetermined time the CH_4 supply was terminated and the reactor was flushed with N_2 for 30 min. Because of the time needed to completely flush out the remaining CH_4, H_2, and CO in the reactor system and the fact that the remaining gases continued to participate in the reduction of tungsten oxides, analysis of effluent gas continued even after the CH_4 supply was stopped. Next, water splitting was performed at the same temperature for an appropriate time by introducing water. The flow rate of liquid water corresponded to a steam flow rate of 7 cm^3 (STP)/min, and N_2 was used as the carrier gas at a flow rate of 13.5 cm^3 (STP)/min. Effluent gas during methane reforming or water splitting was analyzed by the same gas chromatographs employed during TPR. After water splitting, the reactor was flushed with N_2 for 30 min, and the methane reforming-water splitting cycle was repeated.

5. Sample Characterization

Fresh samples and samples obtained after cyclic operations were analyzed by X-ray diffraction (XRD: D8 Focus, Bruker AXS, Germany) and scanning electron microscopy (SEM: JSM7000F, Jeol, Japan). The surface areas of the fresh samples and the samples obtained after the reaction were measured with an N_2 adsorption apparatus (Micromeritics ASAP 2020, US). The content of WO_3 in the fresh samples was analyzed by X-ray fluorescence spectroscopy (XRF: S4, Bruker, Germany).

DETERMINATION OF THE EXTENT OF REDUCTION

The definitions of the extent of reduction, yield, and overall degree of WO_3 reduction are the same as previously described [1]. In the first stage of methane reforming, the following reduction reactions can occur [21-24].

$$WO_3+CH_4 \rightarrow WO_2+2H_2+CO \quad (1)$$

$$WO_3+H_2 \rightarrow WO_2+H_2O \quad (2)$$

$$WO_3+CO \rightarrow WO_2+CO_2 \quad (3)$$

In the second stage, produced WO_2 is reduced to metallic W by methane as well as H_2 and CO:

$$WO_2+2CH_4 \rightarrow W+4H_2+2CO \quad (4)$$

$$WO_2+2H_2 \rightarrow W+2H_2O \quad (5)$$

$$WO_2+2CO \rightarrow W+2CO_2 \quad (6)$$

Other main competing reactions are [1]:

$$CH_4 \rightarrow C+2H_2 \quad (7)$$

$$2C+WO_2 \rightarrow 2CO+W \quad (8)$$

The extent of each reduction reaction, ξ_i, is defined as follows:

$$\xi_i=(\text{moles of } WO_3 \text{ reduced to } WO_2 \text{ by Reaction i})/(\text{moles of loaded } WO_3),\ i=1\sim3 \quad (9)$$

$$\xi_i=(\text{moles of } WO_2 \text{ reduced to W by Reaction i})/(\text{moles of loaded } WO_3),\ i=4\sim6 \quad (10)$$

Then,

$$\xi_1+\xi_2+\xi_3 \le 1 \quad (11)$$

$$\xi_4+\xi_5+\xi_6 \le 1 \quad (12)$$

The yields of H_2, CO, and CO_2 obtained during the methane reforming step are defined as the molar ratios of all H_2, CO, and CO_2 produced during a specified experiment relative to the amount of WO_3 in the sample, respectively. Let the yields of H_2, CO, and CO_2

be a, b, and c mol/mol WO_3, respectively. Then, if methane decomposition (reaction 7) is negligible, the following relations between a, b, c, and ξ_i can be obtained.

$$a=2\xi_1-\xi_2+4\xi_4-2\xi_5 \quad (13)$$

$$b=\xi_1-\xi_3+2\xi_4-2\xi_6 \quad (14)$$

$$c=\xi_3+2\xi_6 \quad (15)$$

In our previous study [1], reactions 1 to 3 were confirmed to occur predominantly in the first stage while the amount of formed W was quite small. Let the yields of H_2, CO, and CO_2 in the first stage be a′, b′, and c′ mol/mol WO_3, respectively. Based on the observation of negligible W formation, the following relations are thus obtained.

$$\xi_1=b'+c' \quad (16)$$

$$\xi_2=2(b'+c')-a' \quad (17)$$

$$\xi_3=c' \quad (18)$$

Therefore, ξ_1, ξ_2, and ξ_3 can be estimated from measured a′, b′, and c′, respectively, resulting in the following relationship:

$$\xi_1+\xi_2+\xi_3=1=3b'+4c'-a' \quad (19)$$

The point at which Eq. (19) is satisfied can be found from measurements of a′, b′, and c′, and the corresponding ξ_1, ξ_2, and ξ_3 can be calculated. This allows ξ_4, ξ_5, and ξ_6 to be estimated from a, b, and c using Eqs. (13)-(15), respectively.

The overall degree of reduction of WO_3 is defined as follows:

$$\text{Overall degree of } WO_3 \text{ reduction (\%)} = [(1/3)\times(\text{moles of consumed lattice oxygen atoms})/(\text{moles of loaded } WO_3)]\times 100 \quad (20)$$

This value can be calculated from a, b, and c by using a material balance. If all WO_3 is reduced only to WO_2 without forming W, the overall degree of WO_3 reduction is 33.3%.

During water splitting of the reduced sample, H_2O oxidizes WO_2 and W to WO_3 to produce H_2 [1,21-24]. If deposited carbon is present, CO can be produced by oxidation with H_2O; furthermore, a portion of CO can be oxidized to CO_2 [1]. The H_2, CO, and CO_2 yields during water splitting are defined respectively as follows: (moles of produced H_2, CO, and CO_2)/(moles of loaded WO_3).

RESULTS AND DISCUSSION

1. TPR Experiments

The programmed temperature rise up to 1,273 K and production rates of H_2, CO, and CO_2 from the 10 wt% WO_3/n-ZrO_2 sample during TPR are shown in Fig. 2. The experiment was continued until the production of CO or H_2 became negligible. Generation of H_2 was detected starting from 873 K, which was 80 K higher than the temperature observed for 10 wt% WO_3/μ-ZrO_2 [1]. This is likely due to a stronger interaction between the high-surface-area support and smaller particles of WO_3. Until the temperature reached ~1,035 K, the produced gases consisting primarily of H_2 and CO were in trace amounts, which was similar to the observation for 10 wt% WO_3/μ-ZrO_2 [1]. Thus, the actual amounts detected were somewhat uncertain due to detection limitations. The production rates of H_2 and CO increased until the temperature reached 1,273 K, after which production of H_2 and CO decreased rapidly, and then production of CO and H_2 became negligible after 35 and 60 min, respectively. Production of CO_2 was observed starting from 1,035 K and became negligible at ~1,200 K.

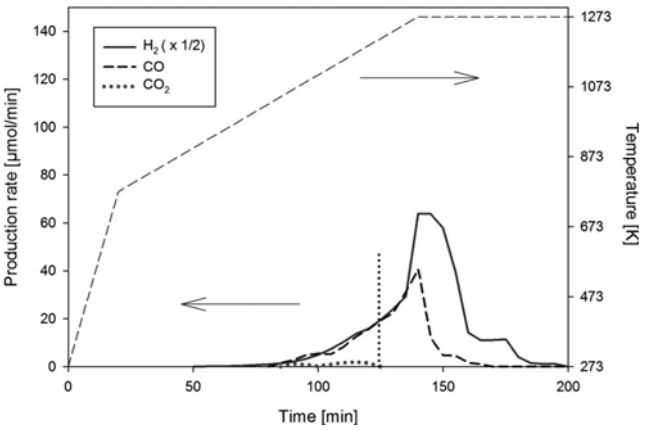

Fig. 2. Production rates of H_2, CO, and CO_2 during TPR of the 10 wt% WO_3/n-ZrO_2 sample (The vertical dotted line indicates the point where Eq. (19) is satisfied; this point is also shown in the following figures for methane reforming.).

The results described above were largely similar to those in our previous study [1], and thus can be explained similarly. To reiterate, the process of reduction in the methane reforming step can be divided into three stages: (I) reduction of WO_3 to WO_2, (II) reduction of WO_2 to W, and (III) significant methane decomposition. The end of the first stage was determined by identifying the point that satisfied Eq. (19), and estimates of ξ_1, ξ_2 and ξ_3 were subsequently determined. This point was found at around 125 min of running time (1,200 K), where a′=1.644, b′=0.758, c′=0.093, ξ_1=0.850, ξ_2=0.057, and ξ_3=0.093 mol/mol WO_3. That is, until this point, 5.7% and 9.3% of WO_3 was reduced to WO_2 by the produced H_2 and CO, respectively. The $H_2/(CO+CO_2)$ ratio was 1.93, indicating that the contributions of reduction by H_2 and CO were relatively small. The point at which the H_2/CO ratio started to rapidly increase from 2 was determined as the starting point of the third stage.

From the start of the experiment to the end of the second stage (at 1,260 K), the obtained yields were as follows: a=2.775, b=1.310, and c=0.093 mol/mol WO_3. The entire $H_2/(CO+CO_2)$ ratio was 1.98 and the overall degree of WO_3 reduction was 51.8%. Based on these measurements, the extent of reduction in the second stage was calculated as follows: ξ_4=0.276 and ξ_6=~0 mol/mol WO_3, indicating that only 27.6% of WO_2 was reduced to W solely by methane with negligible contributions of H_2 and CO. The $H_2/(CO+CO_2)$ ratio in the second stage was 2.05, which indicated that a small amount of H_2 was also produced by methane decomposition (reaction 7), and thus ξ_5 could not be calculated from the measured hydrogen yield [1].

The sharp increase in H_2 production in the next stage indicated rapid methane decomposition. This was most likely due to metallic W covering the outer surface of tungsten-oxides particles, which is known to facilitate methane decomposition [1]. Because of the accompanying carbon deposition on solid surfaces, which in turn inhibited the facilitating action of W, the rate of methane decomposition decreased rapidly within a short time. The CO production during

Table 1. Summary of TPR results

Sample	10 wt% WO_3/n-ZrO_2	10 wt% WO_3/μ-ZrO_2 [1]	30 wt% WO_3/n-ZrO_2	50 wt% WO_3/n-ZrO_2
End of 1st stage (running time [min] and temp. [K])	125, 1200	130, 1273	134, 1247	147, 1273
End of 2nd stage (running time [min] and temp. [K])	135, 1260	150, 1273	165, 1273	200, 1273
ξ_1 (mol/mol WO_3)	0.850	0.608	0.520	0.506
ξ_2 (mol/mol WO_3)	0.057	0.282	0.406	0.398
ξ_3 (mol/mol WO_3)	0.093	0.110	0.074	0.098
ξ_4 (mol/mol WO_3)	0.276	0.560	0.432	0.398
ξ_5 (mol/mol WO_3)	NE[a]	0.193	0.259	0.235
ξ_6 (mol/mol WO_3)	0	0.045	0.051	0.060
$\xi_4+\xi_5+\xi_6$ (mol/mol WO_3)	0.276	0.798	0.742	0.693
$H_2/(CO+CO_2)$ ratio in 1st stage	1.93	1.54	1.22	1.22
$H_2/(CO+CO_2)$ ratio in 2nd stage	2.05	1.65	1.40	1.41
$H_2/(CO+CO_2)$ ratio in 1st & 2nd stages	1.98	1.61	1.33	1.33
Consumption of lattice oxygen to the end of 2nd stage (mol O/mol WO_3)	1.55	2.61	2.48	2.39
Overall degree of WO_3 reduction (%)	**51.8**	**86.7**	**82.8**	**79.6**

[a]Not estimated because the $H_2/(CO+CO_2)$ ratio was higher than 2, but this value was assumed to be negligible

this stage was primarily attributed to reaction of the deposited carbon with WO_2 (reaction 8), and its rate decreased rapidly, which is a common feature of solid-solid reactions exhibiting poor contact between solid reactants. Direct reduction of WO_2 by methane, H_2, and CO was likely negligible during this stage due to inhibition of contact between gases and WO_2 by the deposited carbon [1]. The overall degree of WO_3 reduction calculated from the produced CO to the end of this experiment was 82.8%.

On the other hand, there were considerable differences when compared with 10 wt% WO_3/μ-ZrO_2 [1] as shown in Table 1. First, the overall reduction rate was faster for the WO_3/n-ZrO_2 sample, evidenced by the time taken either to the end of the first stage or to the end of the second stage. Second, the contributions of H_2 and CO to the reduction of both WO_3 and WO_2 were significantly less for the WO_3/n-ZrO_2 sample, resulting in an $H_2/(CO+CO_2)$ ratio much closer to 2. This result was attributed to the faster reduction rate, which allowed for the reduction to be completed at a lower temperature, well below 1,200 K for the first stage and below 1,260 K for the second stage. For the WO_3/μ-ZrO_2 sample, the second stage ended 10 min after the temperature reached 1,273 K. In addition, it was observed that the $H_2/(CO+CO_2)$ ratio was closer to 2 as the temperature decreased below ~1,200 K [1]. Third, production of CO_2 was negligible shortly after the end of the first stage, while for the WO_3/μ-ZrO_2 sample CO_2 production continued to the end of the second stage.

The production rates of gases during TPR of the 30 wt% WO_3/n-ZrO_2 sample are shown in Fig. 3. For brevity, a graph for the 50 wt% sample is not shown because it was similar to that for the 30 wt% sample. The results obtained for TPR of the 30 and 50 wt% samples are summarized in Table 1. The trends were in essence similar to those of the 10 wt% WO_3/n-ZrO_2 sample, but there were some differences. Specifically, the duration of the first and second stages increased as the WO_3 content increased due to the larger amount of WO_3 [1]. The extent of reduction by H_2 in the first stage, ξ_2, was markedly increased to 0.406 and 0.398 for the 30 and 50 wt% samples, respectively. This result indicated that the rate of reduction of WO_3 to WO_2 by H_2 was increased, and thus the $H_2/(CO+CO_2)$ ratio in the first stage decreased considerably as the WO_3 content increased. There are two primary reasons for this effect: the temperature level during reduction of higher-content samples was higher, and the higher-content samples had more remaining WO_3, which provided a greater opportunity for H_2 to participate in reduction [1]. However, the extent of reduction by CO did not change significantly, which was similar to the observation for the WO_3/μ-ZrO_2 samples [1]. During the second stage, the production rates of H_2 and CO remained nearly constant, probably due to the nearly constant temperature. The production of CO_2 was extended to the end of the second stage, again due to the larger amount of WO_2 produced from WO_3 and the higher temperature, which provided a significantly higher chance for CO to react with WO_2. Thus, the extent of reduction by H_2 and CO was significant, with relative contributions of H_2 and CO (i.e., $\xi_5/(\xi_4+\xi_5+\xi_6)$ and $\xi_6/(\xi_4+\xi_5+\xi_6)$) towards the reduction of WO_2 to W of 34-35% and 7-9%, respectively. As a consequence, the $H_2/(CO+$

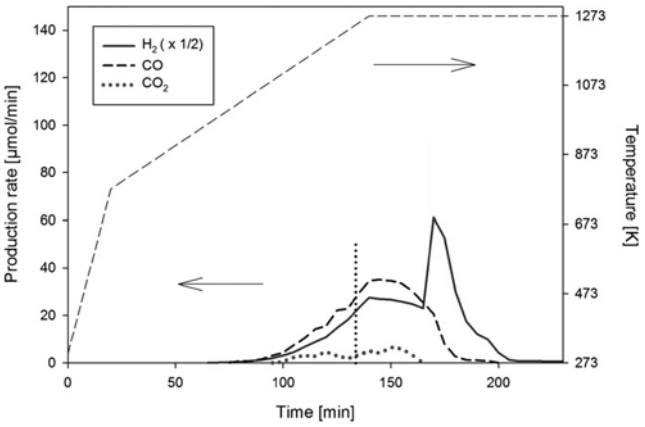

Fig. 3. Production rates of H_2, CO, and CO_2 during TPR of the 30 wt% WO_3/n-ZrO_2 sample.

CO_2) ratios in the second stage and the overall ratios were ~1.4 and ~1.3, respectively. Lastly, the degree of WO_2 reduction was similar for the 30 and 50 wt% samples, ranging from 69 to 74%, and the overall degree of WO_3 reduction at the end of the second stage was near 80% for both samples, which was much higher than that for the 10 wt% sample.

2. The First Cycle of Methane Reforming and Water Splitting at Constant Temperature

The results of our previous study indicate that the suitable operating temperature for WO_3 samples ranges from ~1,200 to 1,273 K [1]. Thus, the experiments in this study were performed at two fixed temperatures, 1,223 and 1,273 K. First, the ending time of the second stage was determined for each set of samples and temperatures during a long reaction run, after which the samples were collected and subjected to water splitting. Because the results were similar to those of our previous study [1] as shown in Fig. 3, they are only briefly summarized here as follows. Production of CO_2 was observed to the end of the second stage during methane reforming, generation of CO and CO_2 was observed during subsequent water splitting, and removal of remaining carbon during water splitting was ~80%: this removal was calculated by following the procedure described in Ref. [1]. The percent removal in this study was somewhat higher than for the WO_3/μ-ZrO_2 sample (65%) [1], but nevertheless indicated that a significant portion of the deposited carbon could not be removed.

Next, to avoid significant methane decomposition, the methane feed was stopped at the ending time of the second stage, and the reaction and analysis were continued for an additional 25 min while the remaining gases were flushed. The results obtained during methane reforming of the 10 wt% sample at 1,223 K are shown in Fig. 4 and Table 2. The point that satisfied Eq. (19) was identified at approximately 10 min, while the second stage ended at 35 min. These times were considerably shorter than those reported for the 10 wt% WO_3/μ-ZrO_2 sample [1], which was expected based on the TPR results. Because the temperature was higher than the overall temperature level during the first and second stages in the TPR experiment, the degree of WO_2 reduction, $\xi_4+\xi_5+\xi_6$, as well as the overall degree of WO_3 reduction at this temperature was much higher than those obtained during TPR. Likewise, the contributions of H_2 to

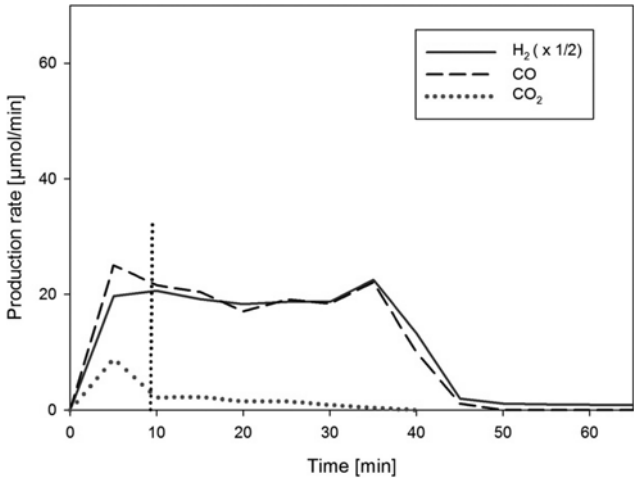

Fig. 4. Production rates of H_2, CO, and CO_2 during methane reforming of the 10 wt% WO_3/n-ZrO_2 sample at 1,223 K.

Table 2. Results of methane reforming and water splitting at constant temperatures with different WO_3 contents for n-ZrO_2-supported and μ-ZrO_2-supported samples

Temperature (K)	1223			1273		
Sample	10 wt% WO_3/ n-ZrO_2	10 wt% WO_3/ μ-ZrO_2 [1]	30 wt% WO_3/ n-ZrO_2	10 wt% WO_3/ n-ZrO_2	10 wt% WO_3/ μ-ZrO_2 [1]	30 wt% WO_3/ n-ZrO_2
End of 1st stage (min running time)	9-13	18	25-28	7-9	12	16-17
End of 2nd stage (min running time)	35	40	90	25	25	50
ξ_1 (mol/mol WO_3)	0.525	0.615	0.462	0.499	0.591	0.445
ξ_2 (mol/mol WO_3)	0.361	0.289	0.425	0.378	0.312	0.447
ξ_3 (mol/mol WO_3)	0.114	0.096	0.113	0.123	0.097	0.108
ξ_4 (mol/mol WO_3)	0.735	0.416	0.450	0.765	0.602	0.445
ξ_5 (mol/mol WO_3)	0.091	NE[a]	0.149	0.236	0.180	0.256
ξ_6 (mol/mol WO_3)	0.044	0.036	0.049	0.063	0.049	0.069
$\xi_4+\xi_5+\xi_6$ (mol/mol WO_3)	0.870	0.452	0.649	1.064	0.831	0.770
$H_2/(CO+CO_2)$ ratio in 1st stage	1.31	1.53	1.28	1.24	1.47	0.99
$H_2/(CO+CO_2)$ ratio in 2nd stage	2.00	2.07	1.70	1.77	1.83	1.45
$H_2/(CO+CO_2)$ ratio in 1st & 2nd stages	1.82	1.84	1.49	1.86	1.71	1.30
Consumption of lattice oxygen to the end of 2nd stage (mol O/mol WO_3)	2.74	1.91	2.30	3.13	2.66	2.54
Overall degree of WO_3 reduction (%)	**91.3**	**63.5**	**76.6**	**104.3**	**88.7**	**84.7**
H_2 yield by water splitting (mol H_2/mol WO_3)	2.43	1.93	2.43	2.51	2.96	2.34
Water splitting time (min)	30	25	50	30	30	45

[a]Not estimated because the $H_2/(CO+CO_2)$ ratio was higher than 2, but this value was assumed to be negligible

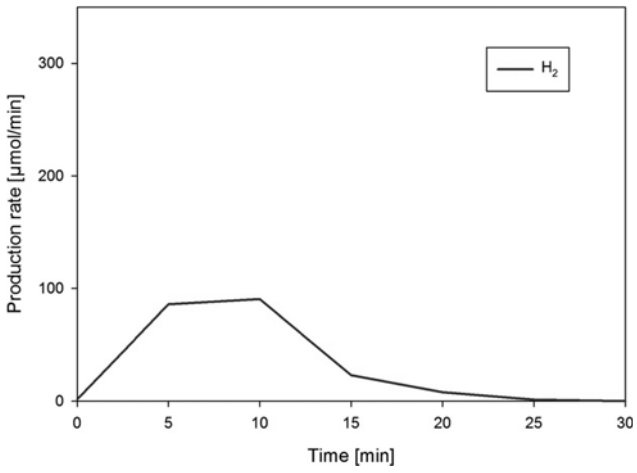

Fig. 5. Results obtained during water splitting of the 10 wt% WO_3/n-ZrO_2 sample at 1,223 K after the experiment shown in Fig. 4.

the reduction during the first and second stages, namely 36.1% and 10.5% (=100×0.091/0.870), respectively, were also much higher. However, the contributions of CO to the reduction were not as prominent. Consequently, the $H_2/(CO+CO_2)$ ratio in the first stage was 1.31 and the overall ratio was 1.82, while the ratio in the second stage was very close to 2.

Next, the 10 wt% WO_3/n-ZrO_2 sample after the methane reforming described above was subjected to water splitting at the same temperature, the results of which are shown in Fig. 5. As expected, no CO was observed. However, the H_2 yield was somewhat smaller than that expected from the overall degree of WO_3 reduction, which is discussed in the following section.

The data for the 10 wt% WO_3/n-ZrO_2 and 10 wt% WO_3/μ-ZrO_2 samples are compared in Table 2. The 10 wt% WO_3/n-ZrO_2 sample showed significantly higher contributions of H_2 to reduction, overall degree of WO_3 reduction, and H_2 yield during the water splitting step than the WO_3/μ-ZrO_2 sample. This result was very likely due to the smaller particle size of tungsten oxides on the higher surface area support.

Table 2 also shows the results for the 30 wt% WO_3/n-ZrO_2 sample. When compared with the 10 wt% WO_3/n-ZrO_2 sample, the contributions of H_2 to the reduction in the first and second stages were increased, and thus the entire $H_2/(CO+CO_2)$ ratio decreased significantly. However, the overall degree of WO_3 reduction was decreased. Again, these results were very likely due to the larger abundance of WO_3 and increased particle size. However, despite changing the support material or WO_3 content, the contribution of CO to the reduction in both stages was not changed significantly. For the corresponding WO_3/μ-ZrO_2 samples, similar trends had also been observed [1].

The data obtained at 1,273 K are presented in Table 2. When compared with the data at 1,223 K, the overall reaction rate and the overall degree of WO_3 reduction were increased. The overall degree of WO_3 reduction for the 10 wt% sample was calculated as slightly higher than 100%, which was considered to be due to errors in measurement [1]. As the temperature increased, increases in the contributions of H_2 and CO to the reduction in the first stage were small, while those in the second stage were significantly higher. These trends were similar to those observed for the WO_3/μ-ZrO_2 samples [1]. Especially, the $H_2/(CO+CO_2)$ ratio in the first stage for the 30 wt% WO_3/n-ZrO_2 sample at 1,273 K was near 1 and the overall ratio was only 1.30. In addition, the H_2 yields obtained by water splitting for the WO_3/n-ZrO_2 samples were again smaller than what was expected based on the overall degree of WO_3 reduction.

The time elapsed to the end of the second stage was not proportional to WO_3 content, which was similar to the results of our previous study [1]. Because longer operating times were required for the higher WO_3-content samples, the production rates of syngas and H_2 were compared. For this comparison, the average production rates of H_2, CO, and CO_2 during methane reforming were calculated. The average rate of WO_3 reduction, defined as the average consumption rate of lattice oxygen atoms in the oxides (mol O/min), was also calculated. Likewise, the average rate of H_2 production during water splitting (mol H_2/min) was calculated. The results of these calculations are presented in Table 3. As expected, the syngas production rate of the WO_3/n-ZrO_2 sample was higher than that of the

Table 3. Average rates of consumption of lattice oxygen, production of H_2, CO, and CO_2 during the first cycle of methane reforming and water splitting

Temperature (K)		1223			1273		
Sample		10 wt% WO_3/n-ZrO_2	10 wt% WO_3/μ-ZrO_2 [1]	30 wt% WO_3/n-ZrO_2	10 wt% WO_3/n-ZrO_2	10 wt% WO_3/μ-ZrO_2 [1]	30 wt% WO_3/n-ZrO_2
Avg. rate during methane reforming	Lattice oxygen consump. (μmol O/min)	33.8	20.6	33.1	54.0	45.9	65.7
	H_2 produc. (μmol H_2/min)	44.7	28.1	29.1	57.6	50.3	44.8
	CO produc. (μmol CO/min)	22.2	13.8	16.5	30.7	27.6	28.2
	CO_2 produc. (μmol CO_2/min)	2.5	1.8	3.1	4.3	3.4	6.4
Avg. rate during water splitting	H_2 produc. (μmol H_2/min)	34.9	33.3	62.9	30.9	51.1	67.3

WO_3/μ-ZrO_2 sample. When the n-ZrO_2-supported samples were compared with each other, the average rate of WO_3 reduction remained similar or slightly increased as the content of WO_3 increased. However, the production rates of H_2 and CO during methane reforming of the 10 wt% WO_3/n-ZrO_2 sample were higher than those of the 30 wt% WO_3/n-ZrO_2 sample at both 1,223 and 1,273 K. This result was the same as for WO_3/μ-ZrO_2 samples, which was attributed to the larger particle size of WO_3 in the higher WO_3-content sample, resulting in slower penetration of reducing gases into larger particles [1]. The production rate of H_2 during water splitting increased about twofold as the WO_3 content increased from 10 to 30 wt%, which was likely due to easier access of H_2O molecules to the reduced oxides through the larger and more abundant pores formed by removal of lattice oxygen atoms during methane reforming. Taken together, these results indicated that the 10 wt% sample was superior to the 30 wt% sample with respect to productivity of syngas and the $H_2/(CO+CO_2)$ ratio. Operation at 1,273 K exhibited higher production rates and shorter reaction periods than at 1,223 K, while the $H_2/(CO+CO_2)$ ratio was much lower than 2. Therefore, selection of the optimum temperature requires a more detailed analysis [1].

3. Repeated Cyclic Operations of Methane Reforming-water Splitting

Based on the above results, the 10 wt% sample and a temperature of 1,223 K were selected to test stability in repeated cyclic operations. Each cycle consisted of methane feeding for a fixed time of 35 min, flushing for 30 min, and water splitting for at least 30 min until the production of H_2 became negligible, which was followed by flushing for 30 min. The results for 10 cycles are shown in Fig. 6. The left-side ordinate in Fig. 6 shows the overall degree of WO_3 reduction, while the right-side ordinate is scaled by the H_2 yield during water splitting, because an overall degree of WO_3 reduction of 100% corresponds to an H_2 yield of 3 mol H_2/mol WO_3 if all reduced oxides are fully re-oxidized.

The overall degree of WO_3 reduction and H_2 yield by water splitting decreased gradually as the cycle number increased, which was similar to the case of WO_3/μ-ZrO_2 samples. However, the H_2 yield by water splitting was considerably less than expected based on the overall degree of WO_3 reduction; it is also notable that the $H_2/(CO+CO_2)$ ratio decreased gradually. Specifically, these two observations are different from those for the WO_3/μ-ZrO_2 sample [1]. The most plausible reason for this difference was the relatively rapid sintering of n-ZrO_2 and WO_3 particles. Moreover, a part of WO_3 could have become embedded in the sintered n-ZrO_2, and thus it could not be re-oxidized; evidence of sintering is presented in the following section.

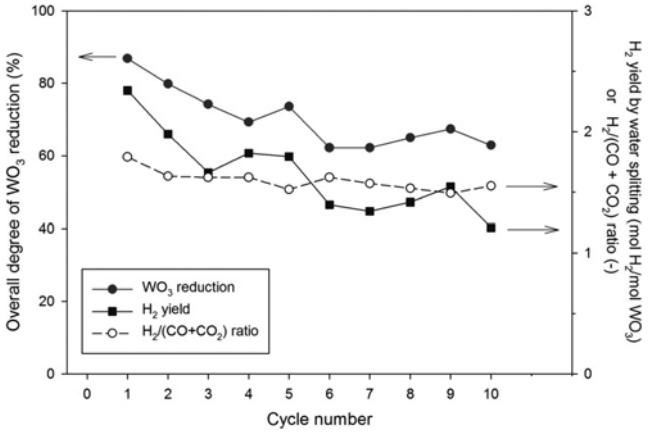

Fig. 6. Results of repeated cyclic operation at 1,223 K for the 10 wt% WO_3/n-ZrO_2 sample: the overall degree of WO_3 reduction, H_2 yield by water splitting, and $H_2/(CO+CO_2)$ ratio.

Detailed data for the cyclic operations are given in Table 4, which strongly supports the reason affirmed above. As cycles were repeated, the operating times to the end of the first stage and for the water splitting increased from 12 and 30 min at the first cycle to 18 and 40 min at the 10th cycle, respectively. As a consequence, the overall degree of WO_3 reduction decreased with a fixed time of methane feeding. Another remarkable observation was that the $H_2/(CO+CO_2)$ ratio in the second stage decreased considerably while ξ_i's in the first stage remained nearly constant. These results were attributed to the gradual increase in WO_3 particle size, consistent with the points discussed above.

4. Characterization Results

The WO_3 loadings determined by XRF in the fresh 10 and 30 wt% samples were 10.1 and 30.5 wt%, respectively. Because the

Table 4. Results during 10 cyclic operations on the 10 wt% WO_3/n-ZrO_2 sample at 1,223 K

Cycle number	1	2	4	6	8	10
End of 1st stage (min running time)	**12**	**12**	**14**	**16**	**16**	**18**
ξ_1 (mol/mol-WO_3)	0.503	0.490	0.530	0.547	0.540	0.569
ξ_2 (mol/mol-WO_3)	0.383	0.408	0.379	0.376	0.382	0.339
ξ_3 (mol/mol-WO_3)	0.114	0.102	0.091	0.076	0.078	0.092
ξ_4 (mol/mol-WO_3)	0.667	0.547	0.398	0.339	0.326	0.309
ξ_5 (mol/mol-WO_3)	0.104	0.113	0.110	0.072	0.119	0.118
ξ_6 (mol/mol-WO_3)	0.031	0.037	0.030	0.022	0.029	0.017
$\xi_4+\xi_5+\hat{\imath}_6$	0.802	0.698	0.539	0.433	0.474	0.444
$H_2/(CO+CO_2)$ ratio during 2nd stage	2.00	1.84	1.85	1.87	1.72	1.67
Overall $H_2/(CO+CO_2)$ ratio	1.79	1.63	1.62	1.62	1.53	1.55
Degree of WO_3 reduction (%)	**86.8**	**79.8**	**69.3**	**62.2**	**65.0**	**62.9**
Water splitting time [min]	30	30	35	40	35	40
H_2 yield by water splitting (mol-H_2/mol-WO_3)	**2.34**	**1.98**	**1.82**	**1.40**	**1.42**	**1.21**

nominal loadings for the samples were in very good agreement with the XRF analysis results, no additional corrections were needed for the numerical data based on the nominal loadings.

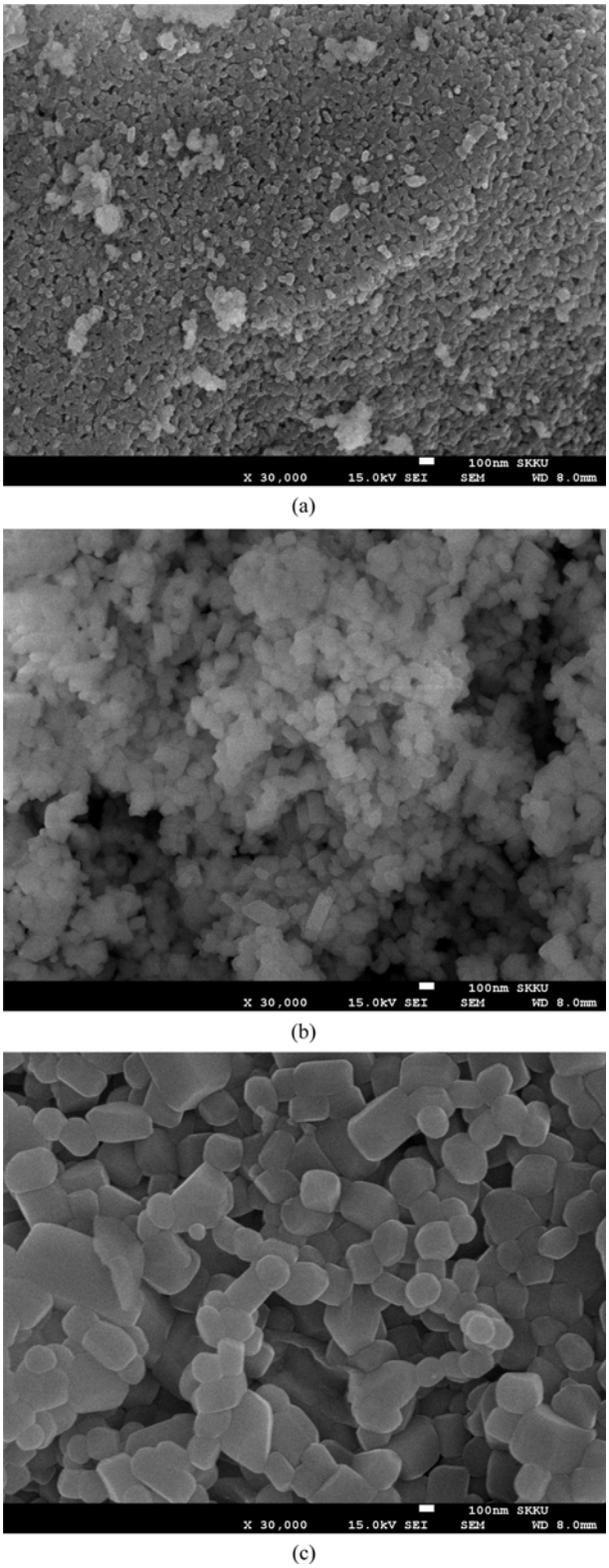

Fig. 7. SEM images of the 10 wt% WO_3/n-ZrO_2 samples: (a) fresh, (b) after the first cycle at 1,223 K, and (c) after 10 repeated cyclic operations (scale bar=100 nm).

SEM images of the samples of fresh 10 wt% WO_3/n-ZrO_2, collected after the first cycle, and after 10 repeated cyclic operations are shown in Fig. 7. The particle size of the fresh sample was 50-100 nm, which was much larger than the 10-30 nm size of pure n-ZrO_2, suggesting that n-ZrO_2 particles agglomerate via the binding action of WO_3. The size of particles increased rapidly with the increasing number of cycles, from 100-300 nm after the first cycle to 300-500 nm after 10 cycles. This result was attributed to sintering of fine particles.

The specific surface areas of the 10 wt% WO_3/n-ZrO_2 samples are presented in Table 5. The specific surface area of the fresh sample was significantly smaller than that of the pure n-ZrO_2 support, further indicating particle agglomeration. After the first reforming by methane, the specific surface area decreased considerably. On the other hand, regardless of whether methane reforming was carried out only to the end of the second stage or extended to a longer time during which there was significant carbon deposition by methane decomposition, the specific surface area remained nearly the same. This means that the deposited carbon exists in thin layers. However, after the first water splitting, the specific surface area decreased further to about 40% of that of the fresh sample, while after 10 cycles,

Table 5. Specific surface areas of the 10 wt% WO_3/n-ZrO_2 samples measured by N_2 adsorption

Samples	Surface area [m^2/g]
n-ZrO_2	51.6
Fresh 10 wt% WO_3/n-ZrO_2	11.3
After 35 min of methane reforming at 1,223 K	7.5
After 80 min of methane reforming at 1,223 K	7.4
After water splitting following methane reforming for 80 min at 1,223 K	4.4
After 10 cycles at 1,223 K	1.6

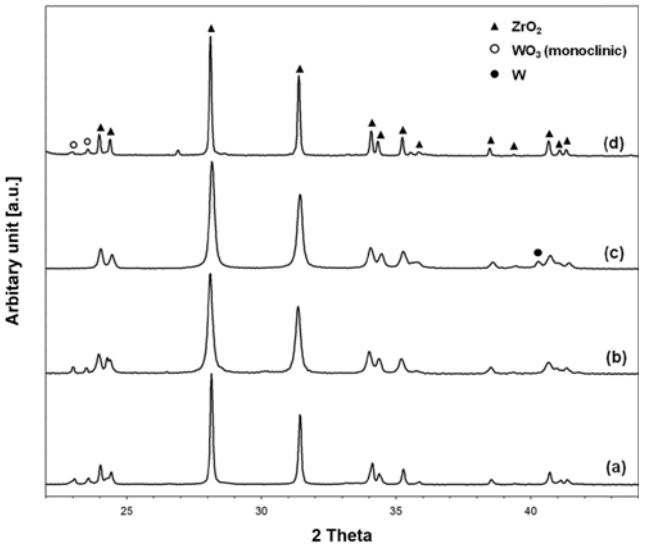

Fig. 8. XRD patterns: (a) fresh 10 wt% WO_3/μ-ZrO_2 [1], (b) fresh 10 wt% WO_3/n-ZrO_2, (c) after the first methane reforming shown in Fig. 4, and (d) after 10 repeated cyclic operations.

the specific surface area was greatly decreased and was similar to that of the WO_3/μ-ZrO_2 sample [1].

XRD patterns of the samples of fresh 10 wt% WO_3/μ-ZrO_2, fresh 10 wt% WO_3/n-ZrO_2, after the first methane reforming, and after 10 repeated cyclic operations are shown in Fig. 8. When comparing fresh samples (Fig. 8(a) and (b)), it was confirmed that the particle size of n-ZrO_2 was significantly smaller than that of μ-ZrO_2, because the peak width is broader for n-ZrO_2 [33]. For the sample after the experiment shown in Fig. 4, WO_3 disappeared and instead metallic W was observed (Fig. 8(c)); WO_2 peaks were not seen clearly, as expected from over 91% of the overall degree of WO_3 reduction (Table 2). For the sample after 10 cycles, the XRD pattern (Fig. 8(d)) was very similar to that for the fresh WO_3/μ-ZrO_2, in good agreement with the SEM and specific surface area data. However, changes of the WO_3 particle size were not clearly identified because the peak intensity for WO_3 was weak. Nevertheless, based on common sense, it is not unreasonable to say that WO_3 particles on a nano-size support are smaller than those on a micron-size support, especially for the fresh samples. If a part of WO_3 was embedded due to relatively rapid sintering of ZrO_2, particles of embedded WO_3 would not grow anymore, remaining in a smaller size. On the other hand, because the WO_3 peaks in Fig. 8(d) appeared weaker and broader than those in Fig. 8(b), it is likely that a part of the exposed WO_3 would form thin layers on the larger ZrO_2 particles.

The results of these characterizations were in good agreement with our points of discussion and affirmed the reaction results reported above. In summary, due to rapid sintering during repeated cyclic operations on nano-size samples, the reaction rates slowed and the $H_2/(CO+CO_2)$ ratio decreased, and eventually the performance of nano-size samples became similar to that of micron-size samples.

CONCLUSIONS

The reduction characteristics of WO_3/n-ZrO_2 during methane reforming were examined, primarily focusing on the effects of particle size of WO_3. WO_3/n-ZrO_2 exhibited reduction characteristics that were essentially similar to those of WO_3/μ-ZrO_2 reported in our previous study [1], namely, (1) the reduction process comprised three stages: (2) the $H_2/(CO+CO_2)$ ratio decreased as the WO_3 content and temperature increased; (3) the syngas production rate decreased as the WO_3 content increased; (4) carbon deposition by methane decomposition could be prevented by controlling the duration of methane reforming; and (5) the overall degree of reduction gradually decreased with the increasing number of cycles.

Some differences were observed when compared with WO_3/μ-ZrO_2 samples. Specifically, the WO_3/n-ZrO_2 samples yielded a higher syngas production rate that resulted in a higher overall degree of WO_3 reduction and a lower $H_2/(CO+CO_2)$ ratio; this resulted from a higher contribution of H_2 to the reduction of tungsten oxides due to the smaller particle size. In addition, the hydrogen yield by water splitting was significantly lower than expected based on the overall degree of WO_3 reduction. Further, the $H_2/(CO+CO_2)$ ratio gradually decreased with the increasing number of cycles, which was primarily due to rapid sintering of WO_3/n-ZrO_2 during repeated cycles. Consequently, WO_3/n-ZrO_2 gradually began to resemble WO_3/μ-ZrO_2. Taken together, the results suggest that WO_3/n-ZrO_2 may not be superior to WO_3/μ-ZrO_2.

ACKNOWLEDGEMENTS

This work was supported by the Career Researcher Program of the National Research Foundation (NRF) of Korea funded by the Ministry of Science, ICT & Future Planning of the Korea government (Grant No.: 2013R1A1A2006167).

NOMENCLATURE

a : H_2 yield during the first and second stages of methane reforming [mol H_2/mol WO_3]
b : CO yield during the first and second stages of methane reforming [mol CO/mol WO_3]
c : CO_2 yield during the first and second stages of methane reforming [mol CO_2/mol WO_3]
a′ : H_2 yield during the first stage of methane reforming [mol H_2/mol WO_3]
b′ : CO yield during the first stage of the methane reforming [mol CO/mol WO_3]
c′ : CO_2 yield during the first stage of the methane reforming [mol CO_2/mol WO_3]
ξ_1 : extent of reduction of WO_3 to WO_2 by methane [mol WO_2/mol WO_3]
ξ_2 : extent of reduction of WO_3 to WO_2 by H_2 [mol WO_2/mol WO_3]
ξ_3 : extent of reduction of WO_3 to WO_2 by CO [mol WO_2/mol WO_3]
ξ_4 : extent of reduction of WO_2 to W by methane [mol W/mol WO_3]
ξ_5 : extent of reduction of WO_2 to W by H_2 [mol W/mol WO_3]
ξ_6 : extent of reduction of WO_2 to W by CO [mol W/mol WO_3]

REFERENCES

1. J. H. Kwak, G. Y. Han and K. J. Yoon, *Int. J. Hydrog. Energy*, **38**, 8293 (2013).
2. A. Kogan, *Int. J. Hydrog. Energy*, **23**, 89 (1998).
3. T. Kodama, S. Miura, T. Shimizu and Y. Kitayama, *Energy*, **11**, 1019 (1997).
4. T. Kodama, *Progr. Energy Combust. Sci.*, **29**, 567 (2003).
5. T. Nakamura, *Solar Energy*, **19**, 467 (1977).
6. M. Lundberg, *Int. J. Hydrog. Energy*, **18**, 369 (1993).
7. A. Steinfeld, A. Frei, P. Kuhn and D. Wuillemin, *Int. J. Hydrog. Energy*, **20**, 793 (1995).
8. S. Abanades and G. Flamant, *Solar Energy*, **80**, 1611 (2006).
9. T. Kodama, Y. Kondoh, R. Yamamoto, H. Andou and N. Satou, *Solar Energy*, **78**, 623 (2005).
10. T. Kodama, N. Gokon and R. Yamamoto, *Solar Energy*, **82**, 73 (2008).
11. S. Abanades, A. Legal, A. Cordier, G. Peraudeau, G. Flamant and A. Julbe, *J. Mater. Sci.*, **45**, 4163 (2010).
12. H. Kaneko, S. Taku, Y. Naganuma, T. Ishihara, N. Hasegawa and Y. Tamaura, *J. Solar Energy Eng.*, **132**, 0212021 (2010).
13. A. Aoki, H. Ohtake, T. Shimizu, Y. Kitayama and T. Kodama, *Energy*, **25**, 201 (2000).
14. V. Galvita, T. Hempel, H. Lorenz, L. K. Rihko-Struckmann and K. Sundmacher, *Ind. Eng. Chem. Res.*, **47**, 303 (2008).

15. C. D. Bohn, J. P. Cleeton, C. R. Müller, S. Y. Chuang, S. A. Scott and J. S. Dennis, *Energy Fuels*, **24**, 4025 (2010).
16. A. M. Kierzkowska, C. D. Bohn, S. A. Scott, J. P. Cleeton, J. S. Dennis and C. R. Müller, *Ind. Eng. Chem. Res*., **49**, 5358 (2010).
17. A. Steinfeld, P. Kuhn and J. Karni, *Energy*, **18**, 239 (1993).
18. A. Steinfeld, M. Brack, A. Meier, A. Weidenkaff and D. Wuillemin, *Energy*, **23**, 803 (1998).
19. K. Otsuka, Y. Wang and M. Nakamura, *Appl. Catal. A*, **183**, 317 (1999).
20. T. Kodama, T. Shimizu, T. Satoh, M. Nakata and K. I. Shimizu, *Solar Energy*, **73**, 363 (2002).
21. K. S. Go, S. R. Son and S. D. Kim, *Int. J. Hydrog. Energy*, **33**, 5986 (2008).
22. K.-S. Kang, C.-H. Kim, W.-C. Cho, K.-K. Bae, S.-W. Woo and C.-S. Park, *Int. J. Hydrog. Energy*, **33**, 4560 (2008).
23. K.-S. Kang, C.-H. Kim, K.-K. Bae, W.-C. Cho, W.-J. Kim, Y.-H. Kim, S.-H. Kim and C.-S. Park, *Int. J. Hydrog. Energy*, **35**, 568 (2010).
24. H. H. Jeong, J. H. Kwak, G. Y. Han and K. J. Yoon, *Int. J. Hydrog. Energy*, **36**, 15221 (2011).
25. T. Kodama, H. Ohtake, S. Matsumoto, A. Aoki, T. Shimizu and Y. Kitayama, *Energy*, **25**, 411 (2000).
26. T. Shimizu, K. Shimizu, Y. Kitayama and T. Kodama, *Solar Energy*, **71**, 315 (2001).
27. T. Kodama, T. Shimizu, T. Satoh and K. I. Shimizu, *Energy*, **28**, 1055 (2003).
28. A. Sim, N. W. Cant and D. L. Trimm, *Int. J. Hydrog. Energy*, **35**, 8953 (2010).
29. J. H. Kwak, Ph.D. Thesis, Sungkyunkwan University (2012).
30. N. F. Fahim and T. Sekino, *Chem. Mater*., **21**, 1697 (2009).
31. L. Guo, J. Zhao, X. Wang, R. Xu and Y. Li, *J. Solid State Electrochem*., **13**, 1321 (2009).
32. J. M. Macak, H. Tsuchiya, A. Ghicov, K. Yasuda, R. Hahn, S. Bauer and P. Schmuki, *Curr. Opin. Solid State Mater. Sci*., **11**, 3 (2007).
33. B. D. Cullity, *Elements of X-ray diffraction, 2nd Ed*., Addison-Wesley, Reading, MA, 102 (1978).